Ruthenium pentamethylcyclopentadienyl mesitylene dimer: a sublimable n-dopant and electron buffer layer for efficient n–i–p perovskite solar cells†

Jorge Avila,[a] Maria-Grazia La-Placa,[a] Elena Longhi,[b] Michele Sessolo,*[a] Stephen Barlow,[b] Seth R. Marder[b] and Henk J. Bolink[a]

-

Electron-transport materials such as fullerenes are widely used in perovskite solar cells to selectively transfer the photogenerated electrons to the electrodes. In order to minimize losses at the interface between the fullerene and the electrode, it is important to reduce the energy difference between the transport level of the two materials. A common approach to reduce such energy mismatch is to increase the charge carrier density in the semiconductor through doping. A variety of molecular dopants have been reported to reduce (n-dope) fullerenes. However, most of them are either difficult to process or extremely air sensitive, with most n-dopants leading to the formation of undesirable side products. Dimers formed by 19-electron organometallic sandwich compounds combine strong reducing ability, clean reactivity, and moderate air stability, while being processable both from solution and in vacuum. In this work, we have investigated the use of pentamethylcyclopentadienyl mesitylene ruthenium dimer, $(RuCp^*mes)_2$, as a dopant for C_{60} in fully vacuum-deposited n–i–p perovskite solar cells. The $(RuCp^*mes)_2$ was either co-evaporated with the fullerene or deposited as a pure thin film on top of the transparent electrode prior to the deposition of the fullerene. It was found that both the co-evaporated blends and the bilayers are effective electron-transport layers, leading to solar cells with efficiencies up to 18%.

Introduction

Lead-halide perovskite solar cells have emerged as a promising alternative thin-film photovoltaic (PV) technology.[1–5] The potential of perovskite PV is demonstrated by the constantly increasing record efficiencies, now exceeding 25%.[6,7] The most efficient perovskite solar cells reported so far have in common the use of TiO_2 as the electron-transport material (ETM).[8,9] These devices are built in an n–i–p architecture, where the ETM is deposited on top of the transparent conductive oxide (TCO) electrode. Some alternative ETMs have been explored, both inorganic – most notably SnO_2 – and organic.[10–14] Among organic semiconductors, fullerene derivatives are widely employed as the ETM in perovskite solar cells, as they provide an ohmic contact with common perovskite absorbers, reducing non-radiative recombination and hysteresis while maintaining a high fill factor (FF).[15–17] In particular, the simplest fullerene, C_{60}, is extensively used in efficient devices and has advantages over chemically modified fullerenes in terms of cost and vacuum processibility.[18–20]

In order to ensure efficient charge extraction from the ETM to the TCO, the alignment of their energy levels and hence a low energetic barrier at the interface is crucial. The large energy difference between the electron affinity of C_{60} and the work function of ITO results in a Schottky barrier height of about 0.8 eV, which leads to a non-ohmic interface, limiting the charge extraction. A common approach to reduce the energy mismatch between a semiconductor and an electrode, and thus reduce ohmic losses, is to increase the charge-carrier density in the organic semiconductor through doping. As a consequence, the Fermi level in the doped semiconductor will shift towards the filled states, reducing the barrier height and favoring charge transfer.[21] In particular, this can be achieved by depositing a thin layer of n-doped C_{60} in between the intrinsic C_{60} and the TCO.[20] In order to prevent intermixing of the doped and intrinsic C_{60} during processing, which would increase non-radiative recombination at the perovskite/doped ETL interface, sequential vacuum sublimation is the most suitable deposition method.[22]

A variety of molecular dopants have been reported to reduce (n-dope) C_{60} and other fullerenes. Examples of one-electron reducing agents are cobaltocene and $W_2(hpp)_4$;[23,24] however, the first is too volatile for standard high vacuum processing,[25] while the latter is extremely air sensitive. Alternative, more stable reductants include halide salts of organic aromatic cations, from which the corresponding organic radicals can be

[a]Instituto de Ciencia Molecular, Universidad de Valencia, C/ J. Beltrán 2, 46980, Paterna, Spain. E-mail: michele.sessolo@uv.es

[b]School of Chemistry and Biochemistry and Center for Organic Photonics and Electronics, Georgia Institute of Technology, Atlanta, GA 30332, USA

† Electronic supplementary information (ESI) available: Materials and methods, perovskite XRD, optical absorption and SEM. See DOI: 10.1039/c9ta09838k

sublimed,[26,27] hydride-donating molecules,[28,29] alkylamine-containing compounds,[30,31] and tetrabutylammonium salts of halides and other simple anions.[32] Several of these molecules have been applied to fullerene doping in perovskite solar cells, increasing the efficiency as compared to that of devices using undoped C_{60} ETMs. The hydride donor 1,3-dimethyl-2(4-(diphenylamino)phenyl)-2,3-dihydro-1*H*-benzoimidazole has been used for the bulk doping of solution-processed C_{60} ETM films.[33] Sequential solution deposition of C_{60} and poly(allylamine) followed by annealing, leads to n-doping of the ETM as well as to the formation of N–C_{60} covalent bonds.[34] However, some of these dopants can lead to the formation of undesirable side products in addition to the fullerene radical anion,[35–37] while others can only be processed from solution.

Dimers formed by some 19-electron organometallic sandwich compounds (as well as those formed by some organic radicals)[38] combine strong reducing ability, clean reactivity (forming solely the corresponding monomeric cations upon doping), and moderate air stability, while being processable both from solution and in vacuum. In view of these favorable properties, they have been used to n-dope a wide variety of semiconductors, including fullerenes.[38–41] Of most relevance to the present work, a thin layer of one such organometallic dimer – pentamethylrhodocene dimer, $(RhCp^*Cp)_2$ – has been vacuum deposited between FTO and vacuum-deposited ETMs, pinning the Fermi level to the lowest unoccupied molecular orbital (LUMO) of the C_{60}.[42] In this work, we have investigated the use of a similar organometallic compound – pentamethylcyclopentadienyl mesitylene ruthenium dimer,[43] $(RuCp^*mes)_2$ – to dope C_{60} in fully vacuum deposited n–i–p perovskite solar cells. $(RuCp^*mes)_2$ has been shown to passivate traps in C_{60} at low concentration and to change the semiconductor work function and highest occupied molecular orbital (HOMO) position with respect to the Fermi level upon doping.[40] The cells were fabricated using a procedure that was described by some of us previously.[20]

In order to evaluate the potential of $(RuCp^*mes)_2$ as an n-dopant for C_{60} in perovskite solar cells, several devices with different architectures have been fabricated. An intrinsic advantage of vacuum deposition is the possibility of selectively modifying and/or exchanging any layer in the device stack, and of studying the consequences for the device performance. The $(RuCp^*mes)_2$ was either co-evaporated with the C_{60} or deposited as a pure thin film on top of the TCO (indium tin oxide, ITO) prior to the deposition of C_{60}. It was found that both the co-evaporated blend of C_{60}:$(RuCp^*mes)_2$ and the bilayer $(RuCp^*mes)_2/C_{60}$ are effective electron transport layers (ETLs), leading to power conversion efficiencies in the range of 17–18%.

Results

The dimer $(RuCp^*mes)_2$ was synthesized following previously published protocols.[44] We initially examined whether $(RuCp^*mes)_2$ is an effective dopant for C_{60}, looking at the optical absorption spectra and conductivity (Fig. 2) of C_{60} and $(RuCp^*mes)_2$ in different layer configurations. For pure thin films of C_{60} and $(RuCp^*mes)_2$, the measured conductivities are on the order of 10^{-8} S cm^{-1}, as expected for intrinsic and highly pure organic semiconductors. To evaluate the reactivity among the two materials we followed two approaches. In one, both materials were co-sublimed at the same time leading to a homogeneous C_{60}:$(RuCp^*mes)_2$ layer (20 nm, dopant concentration 12.5 wt%). In the other approach we deposited a bilayer formed by a thin film of $(RuCp^*mes)_2$ (2.5 nm) covered by C_{60} (10 nm). In this case the contact and hence the eventual reaction between the materials presumably occurs mainly at the interface between them. In both cases we observed a large increase in conductivity (up to 0.5 S cm^{-1} for the co-deposited film, Fig. 2a), indicating that $(RuCp^*mes)_2$ can indeed efficiently dope C_{60}, even when the materials are in contact only at the interface. This is in agreement with the strong reducing character of $(RuCp^*mes)_2$, which is easily capable of n-doping a large variety of organic semiconductors.[39,45,46] We note, however, that the large conductivity in the latter case might indicate some interdiffusion between the two materials (as neutral molecules and/or ions), although of course the amount

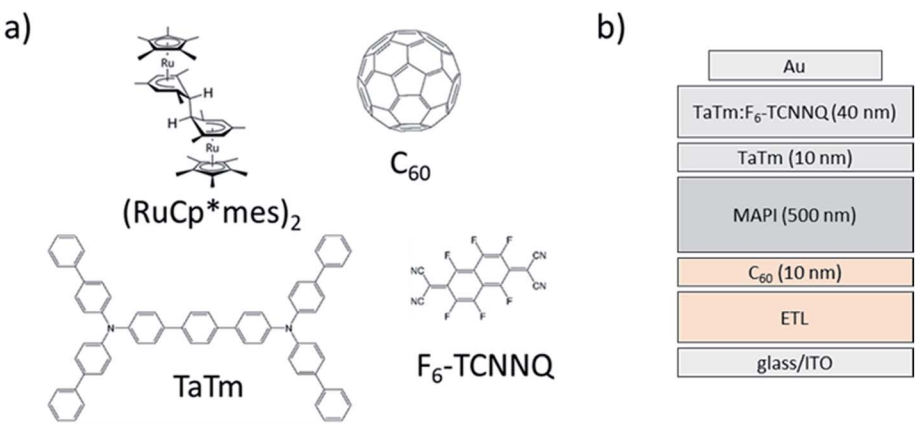

Fig. 1 (a) Chemical structures of transport materials used in the devices. C_{60} is the electron-transport material together with $(RuCp^*mes)_2$ as n-dopant. TaTm is the hole transport material and F_6-TCNNQ is the p-dopant. (b) Schematics of the vacuum-processed perovskite solar cells, where the ETL is either a thin $(RuCp^*mes)_2$ layer or a co-evaporated C_{60}:$(RuCp^*mes)_2$ film.

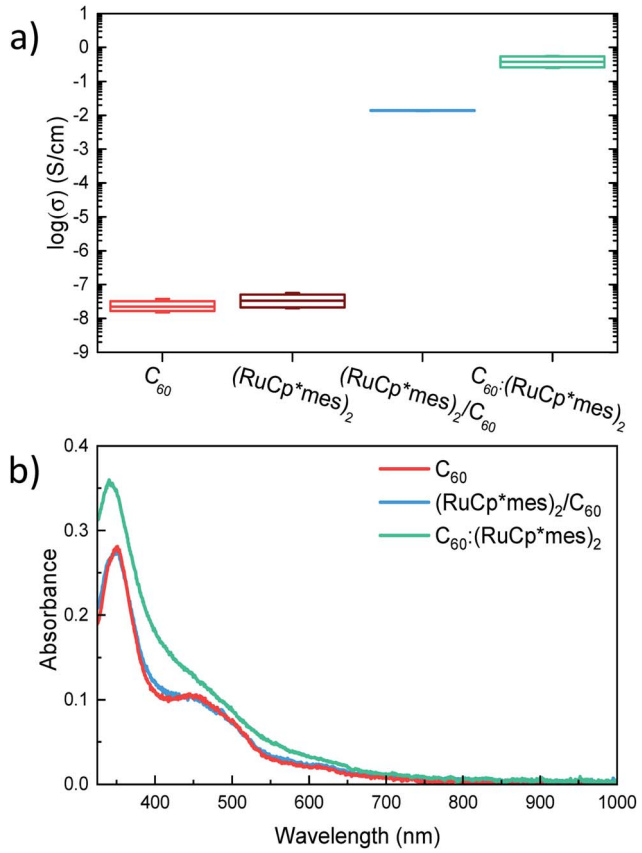

Fig. 2 (a) Conductivity and (b) absorption spectra of different electron transport layers. C_{60}, $(RuCp^*mes)_2$ and C_{60}:$(RuCp^*mes)_2$ films are 10 nm, 2.5 nm and 20 nm thick, respectively.

of the dimers that react and the extent to which dopants diffuse into the C_{60} is not known. From the absorption spectra of C_{60} and of the two doped layers (Fig. 2b) we can observe slightly higher absorbance for the n-doped C_{60} films, with only minor differences between the bi-layer and the co-deposited film. Also, the optical absorption profiles are similar to that of the pure fullerene, without the presence of any new relevant features, indicating that, at these $(RuCp^*mes)_2$ concentration and film thickness, a significant improvement in the conductivity can be obtained without introducing undesirable parasitic absorption.

Thereafter we investigated the performance of the same films in perovskite solar cells. As a first step, we studied devices with the co-sublimed C_{60}:$(RuCp^*mes)_2$ layer. The chosen device architecture was an n–i–p configuration where the ETL is directly deposited on top of the glass/ITO front contact. The layout of the devices is as follows: ITO/ETL/C_{60} (10 nm)/MAPI (500 nm)/TaTm (10 nm)/TaTm:F_6-TCNNQ (40 nm)/Au, where the ETL is a co-evaporated C_{60}:$(RuCp^*mes)_2$ (20 nm), MAPI is methylammonium lead iodide, TaTm is N^4,N^4,$N^{4''}$,$N^{4''}$-tetra([1,1′-biphenyl]-4-yl)-[1,1′:4′,1″-terphenyl]-4,4″-diamine and its p-dopant F_6-TCNNQ is 2,2′-(perfluoronaphthalene-2,6-diylidene)di-malononitrile. The MAPI films were characterized by X-ray diffraction, optical absorption and electron microscopy to verify the material quality. The characterization of a MAPI film (Fig. S1†), together with a detailed description of the device fabrication, can be found in the ESI.†

The current density *vs.* voltage (*J*–*V*) curve for the solar cell employing C_{60} with 12.5 wt% dopant concentration as the ETM shows excellent carrier extraction (FF of approximately 80%) and an open circuit voltage (V_{oc}) of 1.07 V. Together with the short circuit current density (J_{sc}) of 19.8 mA cm^{-2}, these values result in a power conversion efficiency (PCE) of 16.9% (characteristic parameters are reported in Table 1). Decreasing the dopant concentration to 6.25 wt% does not significantly change the FF (81%) or the V_{oc} (only slightly lower at 1.06 V), while it results in a small increase of J_{sc} to 20.6 mA cm^{-2}. Hence the PCE of the cell is enhanced to 17.7%, notably with negligible hysteresis. However, when the dopant concentration is further diminished to 2.5 wt%, the corresponding *J*–*V* curve shows a pronounced s-shape with poor FF (63%), indicative of an inefficient charge collection at the front contact. At this dopant concentration, the C_{60}:$(RuCp^*mes)_2$ layer is no longer able to effectively reduce the interface energy barrier, increasing the recombination losses (V_{oc} is diminished to 1.02 V). The *J*–*V* curve shows also hysteresis between the forward (from short to open circuit) and reverse (from open to short circuit) scans, indicating charge accumulation at the non-ohmic ITO/ETL interface. The observed trend in the FF correlates with the electrical conductivity of the C_{60}:$(RuCp^*mes)_2$ ETL (Fig. 3b), which decreases from about 0.5 S cm^{-1} for a dopant concentration of 12.5 wt% to about 0.05–0.1 S cm^{-1} for the lowest concentration of 2.5 wt%. In comparison with a previous report,[20] the conductivity of the ETL with dopant concentration of 2.5 wt% should be sufficiently high to guarantee efficient charge collection. However, the low performance observed here indicates that this dopant concentration is unable to effectively

Table 1 *J*–*V* parameters of the best devices for each configuration measured under simulated solar illumination; no difference between forward and reverse scans was observed

ETL	Dopant concentration	PCE (%)	V_{oc} (V)	J_{sc} (mA cm^{-2})	FF (%)
C_{60}:$(RuCp^*mes)_2$ (20 nm)	12.5 wt%	16.9	1.07	19.8	80
	6.25 wt%	17.7	1.06	20.6	81
	2.5 wt%	12.5	1.02	19.5	63
Without ETL	—	2.6	0.82	13.6	23
$(RuCp^*mes)_2$ (1 nm)	—	17.1	1.09	20.1	78
$(RuCp^*mes)_2$ (2.5 nm)	—	3.1	0.96	13.5	24

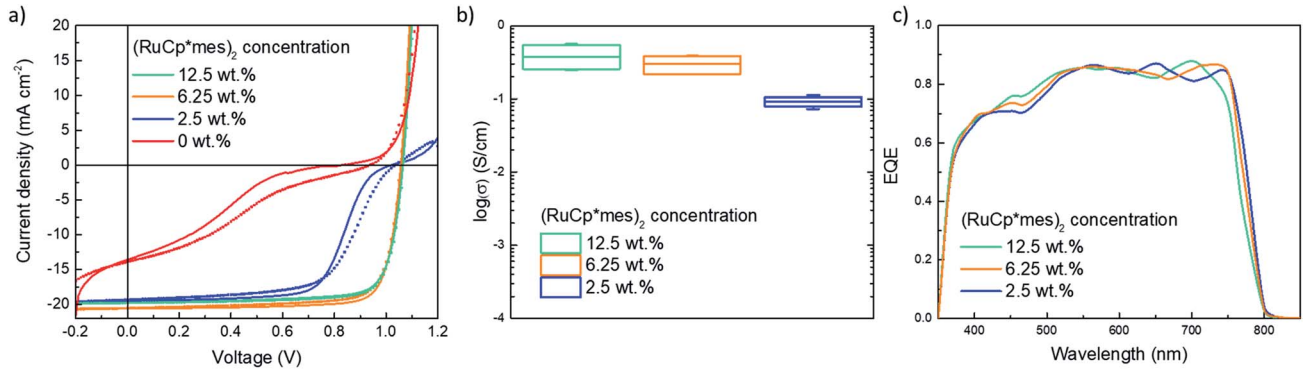

Fig. 3 (a) Representative *J–V* curves measured under simulated 1 sun illumination in forward (straight line) and reverse (dotted line) scan direction for each studied device. (b) Electrical conductivity of the electron-transport layers used in each device. (c) External quantum efficiency (EQE) spectra for the same device series.

reduce the energy mismatch between the ITO and C_{60}, leading to low FF and poorly working devices.

The differences in the current density observed with decreasing dopant concentrations are likely related with different degrees of parasitic absorption due to the doped fullerene. In the external quantum efficiency (EQE) spectra (Fig. 3c), the main feature is a decrease in charge generation around 450 nm when the concentration of dopant is reduced or, in other words, when the relative amount of C_{60} increases. We can correlate the loss in charge generation in the 400–500 nm range with the intense absorption of C_{60} in this spectral region (Fig. 2b). Overall, the EQE spectrum for the device with a dopant concentration of 6.25 wt% leads to the highest integrated current density, in line with the best performance among the device series (Table 1).

We then prepared devices to study the effect of a pure layer of $(RuCp^*mes)_2$ deposited in between the ITO electrode and the C_{60}. The architecture was an n–i–p configuration similar to that previously discussed (ITO/ETL/C_{60} (10 nm)/MAPI (500 nm)/TaTm (10 nm)/TaTm:F_6-TCNNQ (40 nm)/Au). We prepared additional diodes without the dopant interlayer as a reference, where C_{60} is directly in contact with ITO.

The representative *J–V* curves for this device series are represented in Fig. 4a. As expected, the solar cells with the bare ITO/C_{60} front contact shows a very low FF and a low V_{oc} (23% and 0.82 V, respectively). The energy barrier results in non-ohmic charge extraction, reducing the FF and causing non-radiative recombination losses limiting the maximum achievable V_{oc}. Interestingly, when a very thin layer of $(RuCp^*mes)_2$ (1 nm) is introduced between the ITO electrode and C_{60}, the device performance is recovered, with good rectification (FF = 78%) and V_{oc} as high as 1.09 V. Taking into account the photocurrent density (J_{sc} = 20.1 mA cm^{-2}), we obtained a PCE exceeding 17%. We observed performance similar to the cells with n-doped C_{60}, but with an increase in V_{oc} (30 mV) in the case of the pure dopant layer. This indicates that avoiding the use of doped layers can limit the recombination losses leading to enhanced photovoltage. Nevertheless, if the thickness of the thin $(RuCp^*mes)_2$ layer is slightly increased to 2.5 nm, the device shows again hindered charge extraction and low photovoltage, with FF and V_{oc} similar to those measured for the device with only the fullerene as ETM. This behavior suggests a very low electron mobility in the pure $(RuCp^*mes)_2$, which is now essentially blocking the carrier collection. This is somewhat

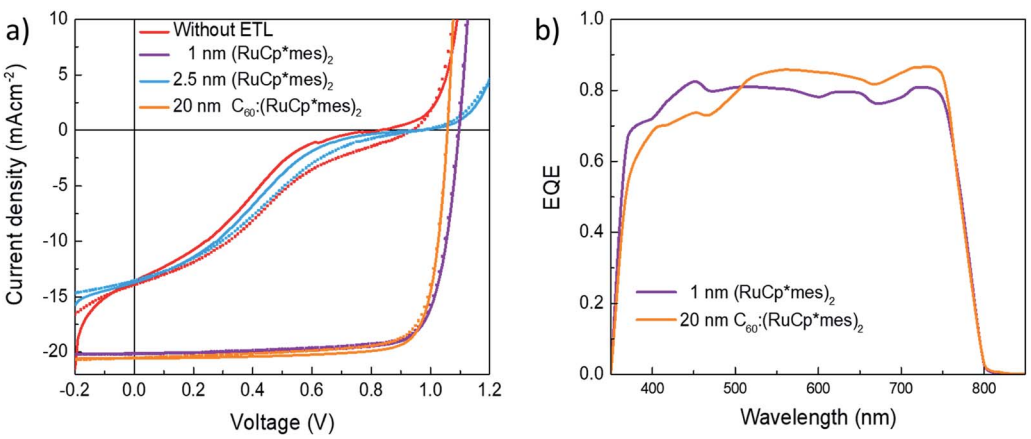

Fig. 4 (a) Representative *J–V* characteristics measured under simulated solar illumination in forward (straight line) and reverse (dotted line) scan direction for devices employing different ETL. (b) External quantum efficiency (EQE) spectra for the devices with $(RuCp^*mes)_2$ and C_{60}-:$(RuCp^*mes)_2$ as the ETL.

different to what was previously observed for $(RhCp^*Cp)_2/C_{60}$, where devices with a nominal interlayer thickness of 10 nm resulted in large V_{oc} and FF.[42] We believe that the differences may originate from different diffusivity of the two organometallic dopants into the C_{60}, as well as from the lower work function of FTO used in the previous work, which would favor electron extraction. In Fig. 4b we can observe similar EQE spectra for the devices using the two types of ETL architectures, the co-evaporated C_{60}:$(RuCp^*mes)_2$ and the bilayer $(RuCp^*mes)_2/C_{60}$, with EQE values of about 0.8 over the whole spectral range, indicating that the small parasitic absorptions (Fig. 1b) have negligible impact on carrier generation. Nevertheless, the device with doped C_{60} exhibits a slightly lower EQE in the blue region of the spectrum. This difference correlates with the ETL thicknesses, as the devices with doped C_{60} have a total ETL thickness of 30 nm resulting in larger parasitic absorption.

Conclusions

In conclusion, we have successfully demonstrated the use of $(RuCp^*mes)_2$ as a n-dopant for C_{60} in vacuum-deposited perovskite solar cells. It was found that both co-evaporated C_{60}:$(RuCp^*mes)_2$ films and $(RuCp^*mes)_2/C_{60}$ bilayers can perform as effective electron-transport layers (ETLs). The simultaneous sublimation of both materials allows to obtain homogeneous layers that form ohmic contact between ITO and the intrinsic fullerene, resulting in efficient and selective charge extraction. Optimization of the dopant concentration allowed the fabrication of solar cells with power conversion efficiency approaching 18%. The thickness of the $(RuCp^*mes)_2$ in the bilayer $(RuCp^*mes)_2/C_{60}$ ETL architecture was found to be critical for the device performance. Very thin dopant layers, around 1 nm, were needed to guarantee efficient charge collection, and resulted in efficiencies exceeding 17%. We observed a higher V_{oc} for solar cells using the bilayer $(RuCp^*mes)_2/C_{60}$ ETL, which is a consequence of the diminished charge recombination compared to doped layers.

Conflicts of interest

There are no conflicts to declare.

Acknowledgements

The research leading to these results has received funding from the European Union's Horizon 2020 research and innovation programme under grant agreement No. 763977 of the PerTPV project. We acknowledge financial support from the the Spanish Ministry of Economy and Competitiveness (MINECO) *via* the Unidad de Excelencia María de Maeztu MDM-2015-0538, MAT2017-88821-R, PCIN-2015-255 and MAT2017-88905-P, the Generalitat Valenciana (Prometeo/2016/135), the U. S. National Science Foundation (DMR-1305247 and DMR-1807797), and the U. S. Air Force Office of Scientific Research (FA9550-18-1-0499). H. B. acknowledges the support of ERA NET PCIN-2017-014. M.S. thanks the MINECO for his RyC contract. J. Á. thanks the Spanish Ministry of Education, Culture and Sport for his pre-doctoral grant (FPU14/04466).

References

1 A. Kojima, K. Teshima, Y. Shirai and T. Miyasaka, *J. Am. Chem. Soc.*, 2009, **131**, 6050–6051.
2 H.-S. Kim, C.-R. Lee, J.-H. Im, K.-B. Lee, T. Moehl, A. Marchioro, S.-J. Moon, R. Humphry-Baker, J.-H. Yum, J. E. Moser, M. Grätzel and N.-G. Park, *Sci. Rep.*, 2012, **2**, 1–7.
3 M. M. Lee, J. Teuscher, T. Miyasaka, T. N. Murakami and H. J. Snaith, *Science*, 2012, **338**, 643–647.
4 T. Leijtens, K. A. Bush, R. Prasanna and M. D. McGehee, *Nat. Energy*, 2018, **3**, 828–838.
5 Z. Li, T. R. Klein, D. H. Kim, M. Yang, J. J. Berry, M. F. A. M. van Hest and K. Zhu, *Nat. Rev. Mater.*, 2018, **3**, 18017.
6 Natl. Renew. Energy Lab., 2019, https://www.nrel.gov/pv/cell-efficiency.html.
7 M. A. Green, Y. Hishikawa, E. D. Dunlop, D. H. Levi, J. Hohl-Ebinger, M. Yoshita and A. W. Y. Ho-Baillie, *Prog. Photovolt: Res. Appl.*, 2019, **27**, 3–12.
8 W. S. Yang, B.-W. Park, E. H. Jung, N. J. Jeon, Y. C. Kim, D. U. Lee, S. S. Shin, J. Seo, E. K. Kim, J. H. Noh and S. Il Seok, *Science*, 2017, **356**, 1376–1379.
9 E. H. Jung, N. J. Jeon, E. Y. Park, C. S. Moon, T. J. Shin, T.-Y. Yang, J. H. Noh and J. Seo, *Nature*, 2019, **567**, 511–515.
10 Z. Zhu, J. Q. Xu, C. C. Chueh, H. Liu, Z. Li, X. Li, H. Chen and A. K. Y. Jen, *Adv. Mater.*, 2016, **28**, 10786–10793.
11 C. Sun, Z. Wu, H. L. Yip, H. Zhang, X. F. Jiang, Q. Xue, Z. Hu, Z. Hu, Y. Shen, M. Wang, F. Huang and Y. Cao, *Adv. Energy Mater.*, 2016, **6**, 1–10.
12 D. Zhao, Z. Zhu, M. Y. Kuo, C. C. Chueh and A. K. Y. Jen, *Angew. Chem., Int. Ed.*, 2016, **55**, 8999–9003.
13 K. Mahmood, S. Sarwar and M. T. Mehran, *RSC Adv.*, 2017, **7**, 17044–17062.
14 S.-H. Turren-Cruz, A. Hagfeldt and M. Saliba, *Science*, 2018, **362**, 449–453.
15 K. Wojciechowski, I. Ramirez, T. Gorisse, O. Dautel, R. Dasari, N. Sakai, J. M. Hardigree, S. Song, S. Marder, M. Riede, G. Wantz and H. J. Snaith, *ACS Energy Lett.*, 2016, **1**, 648–653.
16 D. P. McMeekin, Z. Wang, W. Rehman, F. Pulvirenti, J. B. Patel, N. K. Noel, M. B. Johnston, S. R. Marder, L. M. Herz and H. J. Snaith, *Adv. Mater.*, 2017, **29**, 1607039.
17 J. B. Patel, J. Wong-Leung, S. Van Reenen, N. Sakai, J. T. W. Wang, E. S. Parrott, M. Liu, H. J. Snaith, L. M. Herz and M. B. Johnston, *Adv. Electron. Mater.*, 2016, 1600470.
18 V. O. Eze, Y. Seike and T. Mori, *Org. Electron.*, 2017, **46**, 253–262.
19 D. Liu, Q. Wang, C. J. Traverse, C. Yang, M. Young, P. S. Kuttipillai, S. Y. Lunt, T. W. Hamann and R. R. Lunt, *ACS Nano*, 2018, **12**, 876–883.
20 C. Momblona, L. Gil-Escrig, E. Bandiello, E. M. Hutter, M. Sessolo, K. Lederer, J. Blochwitz-Nimoth and H. J. Bolink, *Energy Environ. Sci.*, 2016, **9**, 3456–3463.

21 K. Walzer, B. Maennig, M. Pfeiffer and K. Leo, *Chem. Rev.*, 2007, **107**, 1233–1271.

22 M. Schwarze, C. Gaul, R. Scholz, F. Bussolotti, A. Hofacker, K. S. Schellhammer, B. Nell, B. D. Naab, Z. Bao, D. Spoltore, K. Vandewal, J. Widmer, S. Kera, N. Ueno, F. Ortmann and K. Leo, *Nat. Mater.*, 2019, **18**, 242–248.

23 F. J. Rizzuto, D. M. Wood, T. K. Ronson and J. R. Nitschke, *J. Am. Chem. Soc.*, 2017, **139**, 11008–11011.

24 T. Menke, D. Ray, J. Meiss, K. Leo and M. Riede, *Appl. Phys. Lett.*, 2012, **100**, 093304.

25 C. K. Chan, F. Amy, Q. Zhang, S. Barlow, S. Marder and A. Kahn, *Chem. Phys. Lett.*, 2006, **431**, 67–71.

26 A. G. Werner, F. Li, K. Harada, M. Pfeiffer, T. Fritz and K. Leo, *Appl. Phys. Lett.*, 2003, **82**, 4495–4497.

27 P. Wei, T. Menke, B. D. Naab, K. Leo, M. Riede and Z. Bao, *J. Am. Chem. Soc.*, 2012, **134**, 3999–4002.

28 F. Li, A. Werner, M. Pfeiffer, K. Leo and X. Liu, *J. Phys. Chem. B*, 2004, **108**, 17076–17082.

29 P. Wei, J. H. Oh, G. Dong and Z. Bao, *J. Am. Chem. Soc.*, 2010, **132**, 8852–8853.

30 S. Fabiano, S. Braun, X. Liu, E. Weverberghs, P. Gerbaux, M. Fahlman, M. Berggren and X. Crispin, *Adv. Mater.*, 2014, **26**, 6000–6006.

31 B. Russ, M. J. Robb, B. C. Popere, E. E. Perry, C. Mai, S. L. Fronk, S. N. Patel, T. E. Mates, G. C. Bazan, J. J. Urban, M. L. Chabinyc, C. J. Hawker and R. A. Segalman, *Chem. Sci.*, 2016, **7**, 1914–1919.

32 C.-Z. Li, C.-C. Chueh, F. Ding, H.-L. Yip, P.-W. Liang, X. Li and A. K.-Y. Jen, *Adv. Mater.*, 2013, **25**, 4425–4430.

33 Z. Wang, D. P. McMeekin, N. Sakai, S. van Reenen, K. Wojciechowski, J. B. Patel, M. B. Johnston and H. J. Snaith, *Adv. Mater.*, 2017, **29**, 1604186.

34 S. Song, R. Hill, K. Choi, K. Wojciechowski, S. Barlow, J. Leisen, H. J. Snaith, S. R. Marder and T. Park, *Nano Energy*, 2018, **49**, 324–332.

35 M. Schwarze, B. D. Naab, M. L. Tietze, R. Scholz, P. Pahner, F. Bussolotti, S. Kera, D. Kasemann, Z. Bao and K. Leo, *ACS Appl. Mater. Interfaces*, 2018, **10**, 1340–1346.

36 B. D. Naab, S. Guo, S. Olthof, E. G. B. Evans, P. Wei, G. L. Millhauser, A. Kahn, S. Barlow, S. R. Marder and Z. Bao, *J. Am. Chem. Soc.*, 2013, **135**, 15018–15025.

37 C. D. Weber, C. Bradley and M. C. Lonergan, *J. Mater. Chem. A*, 2014, **2**, 303–307.

38 B. D. Naab, S. Zhang, K. Vandewal, A. Salleo, S. Barlow, S. R. Marder and Z. Bao, *Adv. Mater.*, 2014, **26**, 4268–4272.

39 S. Guo, S. B. Kim, S. K. Mohapatra, Y. Qi, T. Sajoto, A. Kahn, S. R. Marder and S. Barlow, *Adv. Mater.*, 2012, **24**, 699–703.

40 S. Olthof, S. Mehraeen, S. K. Mohapatra, S. Barlow, V. Coropceanu, J.-L. Brédas, S. R. Marder and A. Kahn, *Phys. Rev. Lett.*, 2012, **109**, 176601.

41 P. J. Smith and C. K. Mann, *J. Org. Chem.*, 1969, **34**, 1821–1826.

42 F. Pulvirenti, B. Wegner, N. K. Noel, G. Mazzotta, R. Hill, J. B. Patel, L. M. Herz, M. B. Johnston, M. K. Riede, H. J. Snaith, N. Koch, S. Barlow and S. R. Marder, *Mol. Syst. Des. Eng.*, 2018, **3**, 741–747.

43 O. V Gusev, M. A. Ievlev, M. G. Peterleitner, S. M. Peregudova, L. I. Denisovich, P. V Petrovskii and N. A. Ustynyuk, *J. Organomet. Chem.*, 1997, **534**, 57–66.

44 H.-I. Un, S. A. Gregory, S. K. Mohapatra, M. Xiong, E. Longhi, Y. Lu, S. Rigin, S. Jhulki, C.-Y. Yang, T. V Timofeeva, J.-Y. Wang, S. K. Yee, S. Barlow, S. R. Marder and J. Pei, *Adv. Energy Mater.*, 2019, **9**, 1900817.

45 S. Guo, S. K. Mohapatra, A. Romanov, T. V Timofeeva, K. I. Hardcastle, K. Yesudas, C. Risko, J.-L. Brédas, S. R. Marder and S. Barlow, *Chem.–Eur. J.*, 2012, **18**, 14760–14772.

46 S. K. Mohapatra, A. Fonari, C. Risko, K. Yesudas, K. Moudgil, J. H. Delcamp, T. V Timofeeva, J.-L. Brédas, S. R. Marder and S. Barlow, *Chem.–Eur. J.*, 2014, **20**, 15385–15394.